Catalysis Today 156 (2010) 76–86

Contents lists available at ScienceDirect

Catalysis Today

journal homepage: www.elsevier.com/locate/cattod

The (electro)catalyst|membrane interface in the Proton Exchange Membrane Fuel Cell: Similarities and differences with non-electrochemical Catalytic Membrane Reactors

Marian Chatenet[a,*], Laetitia Dubau[a], Nathalie Job[b], Frédéric Maillard[a]

[a] Laboratoire d'Electrochimie et de Physico-chimie des Matériaux et des Interfaces (LEPMI), UMR 5631 CNRS/Grenoble-INP/UJF, 1130 rue de la piscine, BP 75, 38402 Saint Martin d'Hères Cedex, France
[b] Université de Liège, Laboratoire de Génie Chimique (B6a), B-4000 Liège, Belgium

ARTICLE INFO

Article history:
Available online 19 March 2010

Keywords:
Proton Exchange Membrane Fuel Cells (PEMFCs)
Utilization factor
Effectiveness factor
Active (catalytic) layer
Platinum
Nafion® ionomer

ABSTRACT

In this paper, we compare the Proton Exchange Membrane Fuel Cell (PEMFC) with non-electrochemical Catalytic Membrane Reactors (CMR). The comparison notably lies on the particular geometry of the membrane|(electro)catalyst interface in PEMFC, the design of which optimizes the triple ionic-electronic-(gas) reactant percolation. Through a selected literature review, we will describe how the performances of practical PEMFC improved following the optimization of (i) the ionomer|electrocatalyst interface and (ii) the mass-transport processes for reactants and products within the Active Layers (AL). We will also focus (iii) on the possible alteration/modification of the intrinsic catalyst electroactivity of Pt/C materials at the ionomer interface and (iv) on the influence of the membrane|electrode architecture and composition on the durability of the PEMFC Membrane-Electrodes Assembly (MEA).

1. Introduction

Catalytic Membrane Reactors (CMRs) are advanced reactors, which synergistically combine the advantages of a catalytic material and a membrane. Three main families of CMR can be distinguished, all displaying specific properties [1,2]. (1) *Extractor* CMR enable increased conversion yields (often beyond thermodynamic equilibrium) and gain in productivity, through the selective removal of one reaction product and the related displacement of the reaction equilibrium. (2) *Distributor* CMR favor sharp selectivity improvements thanks to the distributed feeding of one reactant along the reactor catalytic layer, thereby preventing successive addition reactions by the close control of the reactants concentration within the catalytic layer. It is wise to note that *distributor* CMR may also increase the reactor safety, since they enable a close control of the contact between the reactants, as for *contactor* CMR. (3) *Contactor* CMR improve the wetting between two non-miscible reactant phases and the catalyst, itself immobilized in the porous membrane. A *contactor* CMR actually confines the reaction zone in a region of finite thickness within the membrane. Two configurations of *contactor* CMR are possible. In the *interfacial contactor*, the reactants are supplied on both sides of the catalytic membrane, which sets the interface between the two reactants (where the catalyst is located), thus facilitating the access of the "limiting reactant" to the catalytic site. In opposition, the *forced-flow-through contactor* enables to control the residence time of the reactants within the catalytic layer and to optimize the catalyst/reactant contact (the pore dimensions may be tuned so as to favor the transport mechanism of one reactant interacting with the support wall).

Electrochemical reactors like Proton Exchange Membrane Fuel Cells (PEMFC) are particular (electrochemical) CMR. Like for conventional (non-electrochemical) CMR [1], PEMFC can only reach high performances provided the heart of the cell, the Membrane Electrode Assembly (MEA), is both based on efficient (and well tuned) materials and properly designed [3,4]. The MEA is a multiphase material composed of (i) a Proton Exchange Membrane (PEM), usually a perfluorosulfonated ionomer (PFSI), which acts as both electron insulator and gas separator between the hydrogen and oxygen compartments (as for a *membrane con-*

Abbreviations: AL, active layer (also denoted as CL: catalytic layer); CA, carbon aerogel; CB, carbon black; CX, carbon xerogel; CMR, Catalytic Membrane Reactor; ECSA, electrochemical surface area (cm^2); FER, Fluoride Emission Rate; HOR, hydrogen oxidation reaction; GDE, gas diffusion electrode; GDL, gas diffusion layer; MA, mass activity ($A\,g^{-1}_{Pt}$); MEA, membrane electrode assembly; MPL, microporous layer; NHE, normal hydrogen electrode; NMR, nuclear magnetic resonance; OCP, open-circuit potential (V *vs.* NHE); OCV, open-circuit voltage (V); ORR, oxygen reduction reaction; PAFC, phosphoric acid fuel cell; PEM, Proton Exchange Membrane; PEMFC, Proton Exchange Membrane Fuel Cell; PFSI, perfluorosulfonated ionomer; PTFE, polytetrafluoroethylene; RDE, rotating disk electrode; RH, relative humidity (dimensionless); SA, specific activity ($A\,cm^{-2}_{Pt}$); TEM, transmission electron microscopy; UMEC, ultramicroelectrode with cavity; u_{Pt}, utilization factor (dimensionless); XRD, X-ray diffraction; ε, effectiveness factor (dimensionless).

* Corresponding author. Tel.: +33 476826588; fax: +33 476826777.
E-mail address: Marian.Chatenet@phelma.grenoble-inp.fr (M. Chatenet).

0920-5861/$ – see front matter © 2010 Elsevier B.V. All rights reserved.
doi:10.1016/j.cattod.2010.02.028

tactor CMR [2]), and a transport medium for protons (*extractor* at the anode, *distributor* at the cathode), (ii) two Active Layers (AL), where electrochemical reactions take place and (iii) two Gas Diffusion Layers (GDL), enabling the fuel/oxidant transport, water management and electronic/heat conduction. GDL are often composed of mechanically resistant carbon fibers onto which a so-called MicroPorous Layer[1] (MPL) is deposited, facing the AL. The MPL distributes/evacuates the reactant/products to/from the AL, as detailed in reference [5]. In opposition to the situation in conventional CMR, the reactions taking place in PEMFC are electrochemical reactions that can only occur at the so-called three-phase-boundary between (i) the electrocatalyst particles (usually platinum-based, themselves electronically connected to the current collector through the network of their conducting substrate) and (ii) the ionomer (usually composed of oligomers of the PEM material and providing protons into the volume of the AL) in the presence of (iii) the reactant (H_2 or O_2). Each AL can be compared to a single CMR, into which the ionomer acts as a *distributor* for protons (cathode) and dissolved gases, *contactor* between the gas reactant (O_2 at the cathode, H_2 at the anode), protons, electrons and electrocatalyst particles and *extractor* for the reaction by-products (H^+ at the anode, H_2O at the cathode). Obviously, these three important roles rely on the existence of optimized three-phase boundaries (reactant|ionomer|electrocatalyst interface), which should be distributed to the best possible extent within the volume of the two AL. It is wise to point out here that in PEMFC, the sluggish oxygen reduction reaction (ORR) that takes place at the cathode forbids designing nm-thin electrodes; in contrast the reaction zone should extend on a thickness of a few μm, in which maintaining an optimized triple contact is usually not trivial [3,4].

In the present paper, we will describe how the performances of practical PEMFC improved following the optimization of the ionomer|electrocatalyst interface within the AL at the two electrodes. We will focus on technological limitations related to the design and elaboration of state-of-the-art PEMFC AL regarding the catalyst (i) utilization factor (Sections 2.1 and 3.1) and (ii) effectiveness factor (Sections 2.2 and 3.2), (iii) the modification of the intrinsic catalyst electroactivity at the ionomer interface (Sections 2.4 and 3.3) and (iv) the influence of the MEA architecture/composition on its durability (Section 3.4). For each of the above-mentioned examples, we will emphasize the similarities/differences between PEMFC AL and non-electrochemical CMR. As the terminology used by electrochemists in the field of PEMFC and chemical engineers in the field of CMR may differ, some important definitions and concepts regarding the PEMFC are first detailed in Section 2.

2. Basic definitions and concepts regarding the PEMFC

2.1. The catalyst utilization factor, u_{Pt}

The electrocatalyst *utilization factor* expresses the fraction of Pt-based electrocatalyst nanoparticles that is both in electronic (through the carbon substrate, all the way to the current collector) and ionic (through the ionomer network, all the way to the Proton Exchange Membrane, PEM) connection/percolation in the AL. In other words, u_{Pt} expresses the fraction of electrocatalyst nanoparticles which will be electrochemically active. It is wise to note that u_{Pt} does not take into account the possible mass-transport hindrance for the reactants to reach these electrocatalysts nanoparticles, which is accounted by the *effectiveness factor*, ε (see Section 2.2). More precisely, u_{Pt} can be defined as the ratio of the practical surface area of electrocatalyst to the theoretical surface area of electrocatalyst. The theoretical surface area of electrocatalyst can be derived from physical, chemical or electrochemical measurements (TEM, XRD, H_2 or CO chemisorption are the most common techniques) and corresponds to the number of catalytic sites of the electrocatalyst (*i.e.* the sites at the surface of the electrocatalyst particles). Alternatively, the practical surface area of electrocatalyst, measured for the electrode or the MEA, corresponds to the number of catalytic sites which are both in electronic and ionic percolation. Obviously, the utilization factor depends on the global composition, the nature of the solvent used to disperse the ionomer into the catalytic ink (see Section 2.3) and the intimate mixing of the electrocatalyst powder and ionomer within the electrodes. An experimental definition of the utilization factor was recently given by Gasteiger et al. [6]: u_{Pt} can be determined as the ratio of the electrochemically active surface area measured (*e.g.* using the coulometry of hydrogen desorption or CO-stripping during a cyclic voltammogram, see Section 3.3) in the presence of solid polymer electrolyte to that of the same catalyst but immersed in a liquid electrolyte. It is however wise to note that this experimental definition can yield to an erroneous value of the utilization factor if the electrolyte imperfectly wets the catalytic material.

2.2. The catalyst effectiveness factor, ε

The electrocatalyst *effectiveness factor* is a notion of gas phase heterogeneous catalysis, first introduced by Thiele [7] and Wheeler [8], and later adapted to electrocatalysis for PAFC [9] and PEMFC [10]. In PEMFC, the effectiveness factor can be described as the actual reaction rate (current density, expressed per cm^2 of electrocatalysts) divided by the "theoretical reaction rate" in the absence of ohmic and mass-transport limitations. Obviously, ε accounts for the proton/electron percolation of the Pt electrocatalyst particles (as for u_{Pt}) but also for the mass-transport limitation within the pore texture of the active layers.

It shall be pointed out that confusion can be made regarding the meaning of the term ε. While in chemical engineering, ε usually stands for the void fraction of catalytic beds or catalyst pellets [11], electrochemists in the field of PEMFC use ε for the (electro)catalyst effectiveness factor. Chemical engineers usually employ η to describe this latter term.

2.3. Ink processing

Both the *utilization factor* and the *effectiveness factor* depend on the intimate composition and geometry of the PEMFC AL, which obviously depends on the AL elaboration procedure. In this procedure, an important step is the processing of the electrocatalytic ink. Such ink processing is the necessary homogenization step required to make an intimate blend between the various components of the PEMFC AL. It usually consists of periods of magnetic and/or ultrasonic stirring of the electrocatalyst powder and the ionomer suspension in an appropriate solvent. The interested reader is directed towards reference [12] for more details regarding the preparation steps of PEMFC AL.

2.4. Intrinsic (electro)catalytic activity

The PEMFC electrode reactions, and more specifically the oxygen reduction reaction (ORR), which limits the overall PEMFC efficiency, are surface-sensitive processes [13,14]. Therefore, it is mandatory to compare MEA for Pt/C materials displaying identical morphologies and intrinsic kinetic activities (in the absence of

[1] The microporous layer is actually not a layer only containing micropores in the sense of the IUPAC definition (pores of diameter < 2 nm). Conversely, this blend of carbon black and PTFE contains macropores (pores of diameter > 50 nm, located between the carbon grains and PTFE nodules) so as to enable easy H_2 or O_2 gas and water mass transport from/to the gas channels of the bipolar plates.

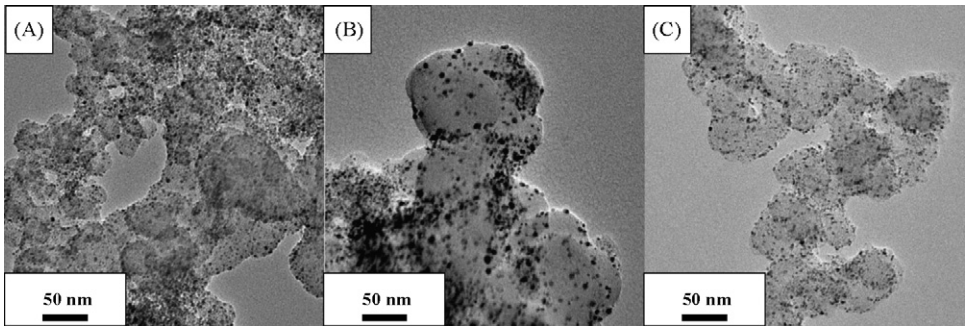

Fig. 1. Effect of ink processing on the Pt morphology for 20 wt.% Pt/Vulcan XC72 (E-Tek)—(A) Magnetic stirring 1 H (B) Ultrasonic treatment 1 H (C) Ultrasonic treatment 5 H.

mass-transport limitation) to be able to draw conclusions on the influence of the pore structure of the AL and related mass-transport hindrance.

The intrinsic (electro)catalytic activity of ORR is often expressed in terms of current density with respect to the mass of electrocatalyst (mass activity, MA) or to the specific (real) area of electrocatalyst (SA), *i.e.* the theoretical area of electrocatalyst, as measured in liquid electrolyte [6] (see Section 2.1). Practically, the MA or SA values can be derived from measurements undertaken in dedicated electrochemical cells, for example in the rotating disk electrode (RDE) setup, either in the thin-film [15–17] or the porous [10,18] configurations. In both techniques, a μm-thick active layer of the desired electrocatalyst is immobilized at the RDE tip, thereby enabling facile correction from mass-transport limitations in the solution using the Levich or Koutecki–Levich methods, as thoroughly described in reference [19]. When the active layer thickness exceeds *ca.* 3 μm, the mass-transport limitation can also proceed in the active layer, especially for potential lower than 0.8 V *vs.* NHE. To avoid such bias when the porous RDE technique is used, the MA and SA values are usually calculated at potential of 0.9 or 0.85 V *vs.* NHE, for which the correction from the oxygen diffusion in solution is sufficient [10,20,21].

Lately another technique, the ultramicroelectrode with cavity (UMEC), was used to characterize Pt/C electrocatalysts. In such setup, the Pt/C powder is immobilized in the cavity of the UMEC, which generally extends on a volume of *ca.* 10–30 μm diameter and height [22]. For a complete description of the UMEC technique and its application for the characterization of (sub)micron-size insoluble powder materials, the reader is referred to [22,23] and references therein. Due to the usual AL thickness in the UMEC technique (*ca.* 10–30 μm), the correction from the oxygen diffusion in the active layer is necessary for both high and low ORR overpotential ($E < 0.8$ V *vs.* NHE and $E > 0.8$ V *vs.* NHE, respectively). Such correction can be obtained using the macro-homogeneous model, as thoroughly described in references [10,22,24].

3. Results and discussion

3.1. From early to state-of-the-art PEMFC electrodes: optimizing the (electro)catalyst|Proton Exchange Membrane interface to reach high Pt utilization factor

PEMFC AL must be designed in order to optimize both the contact between the ionomer and the carbon-supported catalyst particles (so as to reach high values of the utilization factor, u_{Pt} [6], see Section 2.1), and the access of the reactant to the catalytic sites (to enable high catalyst effectiveness factor, ε [10,20], see Section 2.2). As a consequence, not only the materials used, but also the composition of the AL (*e.g.* ratio of Pt/C electrocatalyst to ionomer contents) and preparation technique of the AL influence the MEA performance. As an illustration, it is remarkable to note that, while both the early (1960s) and the present state-of-the-art PEMFC MEA are based on the same materials, *i.e.* Pt electrocatalysts and Nafion® ionomer/Proton Exchange Membrane (PEM), the specific peak power has considerably improved, from *ca.* 2.5 W g^{-1}_{Pt} in the 1960s [3] to *ca.* 1200 W g^{-1}_{Pt} nowadays [6]. Such dramatic improvement resulted from the optimization of the MEA design, composition and elaboration procedures, and rendered possible very high catalyst utilization factor (u_{Pt} beyond 90% is now obtained in state-of-the art electrodes [6,91]) as well as low mass-transport limitations [12]. The figures given above show very clearly that not only the catalytic performance of the carbon-supported Pt-based materials loaded in the AL is important but also the structural arrangement of the MEA (Pt/C, voids for gas reactants, Nafion® ionomer): high performances result from a complex interplay between the pore texture, the electron and proton conductivity, the mass-transport and the electrochemical kinetics [3,4,6]. Obviously, high catalyst utilization factor in PEMFC AL, obtained through optimized ionomer/electrocatalyst contact, can be compared to the mandatory membrane/catalyst contact in *contactor CMR* (see [2] and references therein).

On the one hand, it is well-established that AL materials processing is a key step to obtain homogeneous AL and thus high electrocatalyst utilization factor [25–27] and possibly high specific power [6]. On the other hand, excessive ink processing (see Section 2.3) leads to reduced electrochemically active surface area (ECSA). TEM images of Pt/C nanoparticles + Nafion® ionomer blends obtained after various ink processing procedures (Fig. 1) reveal that ECSA loss correlates with both the agglomeration of Pt nanoparticles on the carbon substrate and the electronic isolation of some Pt nanoparticles. The example of Fig. 1A shows that, whereas 1 H of magnetic stirring maintains a very good dispersion of the Pt nanoparticles over the Vulcan XC72 substrate (a carbon black commonly employed in electrocatalysis), severe agglomeration of the Pt particles into ionomer pockets is obtained after 1 H of ultrasonic treatment (Fig. 1B). The Pt nanoparticles can even be wiped off the carbon substrate, thereby losing their electronic contact with the carbon support, in agreement with the results of Pivovar and colleagues [28,29] (Fig. 2). Surprisingly, after 5 H of ultrasonic treatment (Fig. 1C), the initial Pt/C particles dispersion over the Vulcan XC72 substrate is nearly recovered, probably because such extensive treatment favors the dissolution of the ionomer chains and breaks the ionomer pockets mentioned above.

Let us point out that such ageing of the Pt/C upon ink processing is not witnessed in the absence of (Nafion®) ionomer. The Pt particles trapped in the ionomer pockets are not in contact with the carbon substrate anymore and thus lose the necessary electronic percolation, thereby becoming electrochemically inactive

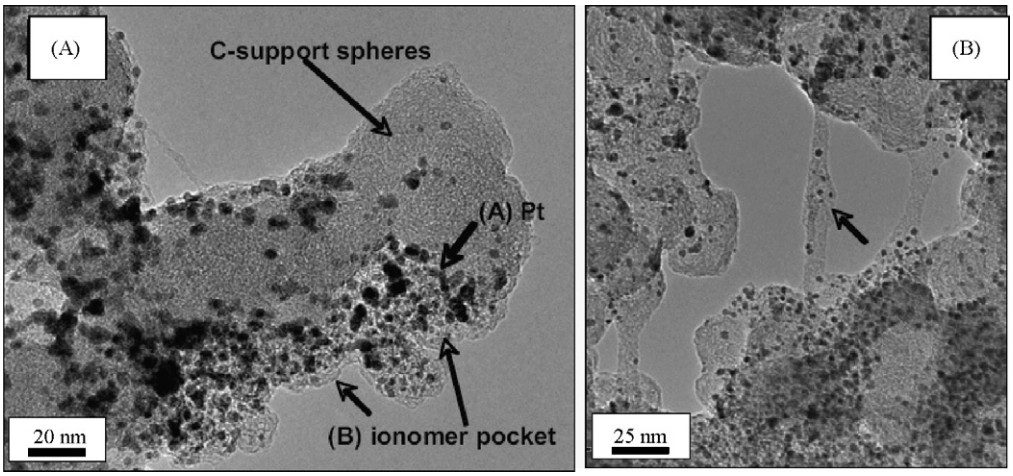

Fig. 2. TEM images showing (A) ionomer pockets that pick up much of the Pt from the surface of the carbon substrate (Vulcan XC72) and (B) ionomer strands that contain isolated Pt particles. Reproduced from Ref. [30] with permission from the Electrochemical Society.

[30]. Such bias does not exist in non-electrochemical CMR, for which the catalysts operate in open-circuit conditions, regardless of any electronic or ionic percolation.

Brosha et al. demonstrated that the effect of the ink processing on Pt/C nanoparticles depends on the chemical nature of the carbon support. They showed improved stability for Pt nanoparticles deposited on a (proprietary) support alternative to the classical Vulcan XC72 carbon black (CB) [29]. In that case, the Nafion® ionomer may even act as a protecting blanket; it plays the dual role of ion-percolator and mechanical protection for the Pt nanoparticles, thus favoring high Pt utilization factor regardless of the ink processing procedure. Such result let us suppose that the carbon structure/morphology and its physico-chemical properties are important parameters to play with in order to improve the electrochemically active surface area of Pt/C. We will see in Section 3.2 that using covalent carbon substrates may also enable to mitigate the issues related to the ink processing and assembling procedures of PEMFC MEA.

Finally, let us also recall some interesting results from Rao et al. in Direct Methanol Fuel Cells [31]. The authors elaborated anode PtRu (1:1) catalysts supported on carbon materials from Sibunit family with BET surface areas ranging from 6 to 415 $m^2\,g^{-1}$. It was observed that u_{Pt} approaches 100% for low surface area supports (*i.e.* with small fraction of both micropores and mesopores with diameter $d < 20$ nm) but dropped down to 10% for the high-surface-area Sibunit carbon supports (with increased amount of micropores and mesopores with $d < 20$ nm). This was explained by the mismatch between the size of the carbon pores and that of the Nafion® micelles. In other words, large Nafion® micelles (>40 nm) cannot enter the pores of $d < 20$ nm, making the three-phase boundary conditions impossible for the PtRu nanoparticles contained inside such pores.

3.2. Towards high (electro)catalyst effectiveness factor ε

As stated in section 3.1, the electrocatalyst particles within a PEMFC electrode operate provided they are in conditions of both electronic (through their electron-conductive support, usually carbon) and ionic (through the ionomer, usually Nafion®) percolation. In that extent, an excess of ionomer can be compatible with high utilization factor: the extreme situation of an "ionomer-plugged" AL (an AL consisting of a 2D network of Pt/C skeleton and ionomer filler) could result in $u_{Pt} = 100\%$ (provided the ink processing is adequate, see Section 3.1). However, it is not guaranteed that 100% of the particles in both ionic and electronic conduction are fully utilized under the dynamic conditions of a PEMFC. A high effectiveness factor ε (see Section 2.2) is also mandatory to reach high power electrical performance. Clearly, ε depends on the pore structure of the AL (and also on the operating conditions), as for a *forced-flow-through contactor CMR* [2]. A proper AL results of a trade-off between sufficient Nafion® content to reach high proton conductivity of the AL (and thus high u_{Pt}) and sufficient porosity to enable high reactant/products mass-transport (and thus high ε), as pointed out in the literature [32–34]. It is worth stressing that the optimal ratio of Nafion® to carbon content found in [32–34] is only valid for the particular carbon substrate used (Vulcan XC72). So, changing (i) the morphology (pore texture) of the carbon substrate used in the AL, (ii) the operating conditions of the PEMFC (low/high humidity of the reactant, low/high temperature, low/high current density) and even (iii) the nature of the reaction at the electrode (*e.g.* slow ORR or methanol oxidation, versus fast hydrogen oxidation reaction (HOR) possibly hindered by the presence of carbon monoxide, a known poison of Pt, in the reformate fuel) requires modifying the AL structure/architecture and thus the catalytic ink composition [12,34–36] and probably the mode of elaboration of the AL.

In that context, we surveyed AL materials of tunable porosity, in order to enable both sufficient ionomer insertion in the volume of the AL and porosity compatible with decreased mass-transport limitations. In that frame, carbon "monolithic" structures,[2] like carbon aerogels (CA) [37,38] or xerogels (CX), are interesting materials because they develop "wide-opened" porosity, in the range of large mesopores (25–35 nm) to small macropores (up to 300 nm) and enable to reach both high u_{Pt} and high ε. Carbon aerogels and xerogels are materials obtained by drying and pyrolysis of organic aqueous gels; the pore texture of these synthetic carbons is easily tailored *via* the synthesis variables of the pristine gel [39,40], as depicted on the example of Fig. 3, related to carbon xerogels.

CA and CX are microporous and meso/macroporous carbons composed of interconnected microporous spherical nodules composing a rigid three-dimensional network. The size of the nodules depends on the synthesis conditions of the gel; the size of the voids located between the nodules (*i.e.* mesopores or macropores) is determined by the size of the nodules and the drying procedure [41]. Fig. 4 [42] shows, in the case of a CA catalyst substrate, how

[2] By "monolithic", we state that the carbon materials retain their pore texture at the micrometric scale, *i.e.* after grinding down to a particle size compatible with catalytic ink preparation. In some case, we used the terms "micromonoliths", the catalytic layer being then composed of 5–20 μm carbon particles [37].

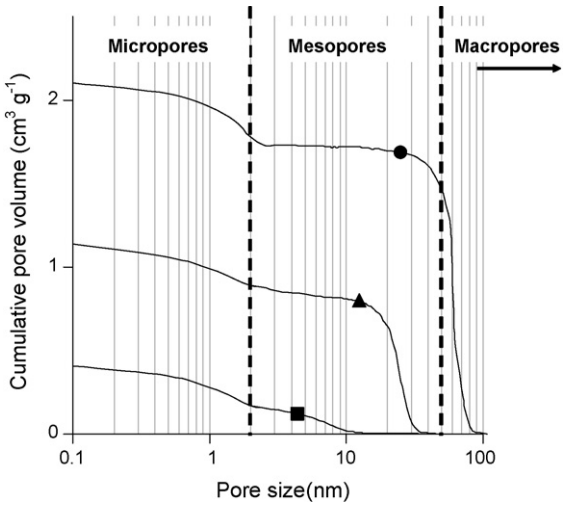

Fig. 3. Pore size distribution of carbon xerogels prepared under various pH conditions, following the method described in reference [40]. (■) pH = 6.25, (▲) pH = 5.75, (●) pH = 5.25.

changing (i) the morphology of the CA (and thus of the AL) at fixed size and shape and thus intrinsic activity of the Pt nanoparticles deposited onto the CA [42–44] and (ii) the ionomer content of the AL, yields very different PEMFC performances (Fig. 4A). Since the electrodes used in this study were elaborated using the same technique (decal method) while exhibited similar Pt loading, Pt intrinsic activity, Pt utilization factor (*ca.* 40–50%) and internal resistances (as measured from electrochemical impedance spectroscopy), the monitored differences in performance only result from different mass-transport hindrance within the volume of the AL [42]: the higher the pore volume and pore diameter of the cathode AL, the more efficient the oxygen mass-transport to the (electro)catalytic sites (Fig. 4B) and thus the better the MEA performances.

Comparable results have been obtained with carbon xerogels [37], which demonstrates that the porosity and the ionomer content of the AL drives the MEA performances, notably in terms of mass-transport, as also monitored for some *diffuser CMR* (see [2,45]). At that point we emphasize that the important parameter to reach high ε is not the pore volume/pore diameter of the original electrode material (*e.g.* Pt/CA or Pt/XC) but that of the AL built from this electrocatalyst and the appropriate ionomer. In that context, it should be mentioned that the assembly of the AL with the Proton Exchange Membrane (PEM) influences both the utilization and effectiveness factors. On the one hand, high u_{Pt} can be reached for thin AL hot-pressed onto the PEM, following the penetration of the AL into the PEM and related improved ionic percolation.[3] On the other hand, thin AL are (in proportion) more intruded by the softened Nafion® during the hot-pressing step, resulting in porosity filling and subsequent larger mass-transport limitations. So, not only the materials and composition of the AL are important to obtain high ε, but also the thickness of the AL and the assembling procedure of the MEA. Similar conclusions were reached by Song et al. [33] for PTFE containing electrodes.

At this point, one should stress that, like in the case of a conventional catalytic bed composed of catalyst pellets piled-up in a reactor, diffusion limitations may originate from different levels of porosities [46]. In particular, an AL prepared from CA or CX materials is composed of three discrete porosity levels:

[3] The penetration of the AL into the PEM is believed to be rather constant, regardless of the AL composition; it would instead depend on the hot-pressing procedure (fixed in this study).

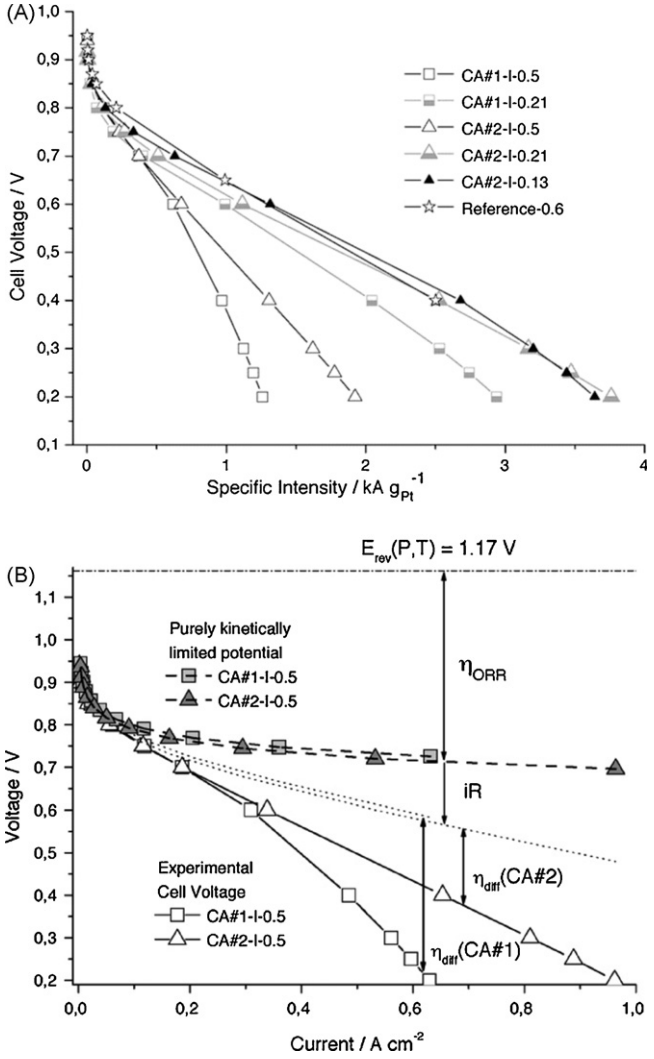

Fig. 4. (A) Specific intensity (kA g^{-1}_{Pt}) of various MEA for 50 cm^2 single cells operated at 70 °C, P_{tot} (H_2/Air) = 1.3/1.3 bar, s (H_2/Air) = 2/2.5 (stoichiometry), RH = 100% (relative humidity) and (B) related voltage losses decomposition revealing the ohmic, kinetic and mass-transport losses for CA#1-I-0.5 and CA#2-I-0.5 MEA. 50 cm^2 single cells were operated at 70 °C, P_{tot} (H_2/air) = 1.3/1.3 bar, s (H_2/air) = 2/2.5 with fully humidified gas (RH = 100%), stoichiometric flows at current density above 0.24 A cm^{-2} and constant flows at current density below 0.24 A cm^{-2}. CA#1 displays pores centred at *ca.* 35 nm, versus 25 nm for CA#2, but active layers made from CA#1 are less "open" than those designed from CA#2, as a result of the larger penetration of Nafion® ionomer in the wider pores. Reproduced from Ref. [42] with permission from Elsevier.

(i) the interparticular voids, *i.e.* the voids between the catalyst particles (micromonoliths), (ii) the intraparticular voids, *i.e.* the meso/macropores located between the carbon nodules and (iii) the intranodular voids, *i.e.* the micropores located inside the carbon nodules. Each level could induce mass-transport limitations, depending on both the pore size and the distance to be covered by the reactants/products within the considered level to reach the active sites. The results presented in Fig. 4A show that, in the case of Pt/CA electrocatalysts, the second level (mesoporosity) clearly regulates the mass-transport: the mesopore size dramatically influences the polarization curve. The same results were obtained with Pt/CX electrocatalysts [37]. Globally, as also shown in the case of a simpler gas phase reaction [46], the intraparticular voids are large enough to avoid diffusion hindrance at this level while the distance to be covered in micropores is too short to induce limitations. However, we point out that in heterogeneous catalysis the problem is generally a bit simpler, as no triple contact is necessary: as a result,

the porosity required for sufficient gas/reactant diffusion into the catalytic layer is not partially obstructed by the ionomer. Indeed, at high Nafion® loading of the AL or in the case of interparticular voids filling during hot-pressing on the membrane, diffusion limitations could shift to the upper level. In the case of Pt/CB catalysts, the second level (intraparticular voids) does not exist and the size of the interparticular voids is much reduced due to the smaller size of the CB particles and aggregates; the mass-transport limitations are thus located at the interparticular level.

The importance of the porosity had already been emphasized for carbon black (CB) based AL [47]. Uchida et al. measured better electrical performance when increasing the specific volume of mesopores of diameter >8 nm covered with the ionomer in the catalyst layer and decreased specific volume of pores less than 8 nm in diameter without ionomer on the carbon surface at the cathode of a PEMFC. Such performance enhancement results from an improved oxygen mass-transport at the cathode.

Finally, it is important to check whether covalent carbon structures like CA and CX are subjected to alteration upon ink processing and MEA hot-pressing (see Sections 2.3 and 3.1). Marie et al. showed that the pore network of Pt/CA was not destroyed during the MEA elaboration. This feature was explained from the flexibility of the CA (micro)monoliths upon compression (as highlighted by Hg-porosimetry measurement): CA monoliths undergo a reversible deformation, at least until a Hg pressure of 500 bar [43]. As a result, the Pt/CA-based AL likely maintains the (controlled) porous structure of the raw Pt/CA materials, even after ink processing and MEA hot-pressing (usual steps of PEMFC MEA elaboration process). Hence, the optimized structure of the AL will decrease diffusion resistances and favor high effectiveness factors. The same results were found with CX [37]: CX, which are denser than CA, were not deformed at all by Hg pressure up to 2000 bar [41]. In opposition, Pt/CB grains are more prone to self "ball-milling" and subsequent detachment of Pt particles upon ink processing and MEA hot-pressing (see Section 3.1), while the pore texture of Pt/CB-based AL depends on the elaboration procedure of the MEA. AL made from high specific surface area CB only display pores of sufficient size to enable efficient mass-transport between the individual CB grains (the grains of high-area CB are usually microporous or mesoporous with small mesopores [48]). Indeed, CB substrates consist of agglomerates which are not covalently bound to each other, so not only the composition of the catalytic ink but also the mechanical steps of AL deposition may influence the AL porous structure: restructuring (irreversible compression) is for example possible during hot-pressing [42], inducing modification of the stacking/packing density of the individual CB grains.

3.3. *Influence of the ionomer on the intrinsic activity of the electrocatalysts*

We have shown in Section 3.1 that the catalytic sites in electrochemical systems like PEMFC are active only provided the ionomer wets the carbon-supported Pt particles. Alternatively, high u_{Pt} may be useless if the remaining porosity of the active layer is not developed enough to enable sufficient reactant/products mass-transport to/from the electrocatalytic sites (Section 3.2). One may also wonder whether this mandatory ionomer|electrocatalyst contact modifies the intrinsic electrocatalytic activity (see Section 2.4) of the catalytic material (usually Pt). We recall that in MEA, the electrocatalyst is used in GDE, the size/volume of which renders extremely awkward to characterize their intrinsic kinetic properties. Indeed, pure kinetic effects may likely be shielded/masked by capacitive, ohmic and mass-transport hindrances, as well documented in references [6,49].

In that context, many research groups do characterize PEMFC electrocatalysts (Pt/C or PtM/C, M = Co, Ni, Cr, Ru, etc.) using simpler AL configurations. They assume that for such simpler geometries, the capacitive and ohmic hindrances can be neglected and the mass-transport limitation easily corrected using mathematical models. The rotating disk electrode (RDE) setup, either in the thin-film [15–17] or the porous [10,18] configurations, is the most popular example. In the former technique, an active layer of the desired electrocatalyst is immobilized in two steps at the RDE tip. First, a layer of electrocatalyst powder is deposited from a suspension in volatile solvent, while a second thin Nafion® layer is added after the solvent evaporation. In the latter, the active layer is deposited in one step from a blend of the electrocatalyst powder and a binder (either Nafion® [10,18,22] or PTFE [24,50–54]). Both techniques require a gentle thermal treatment to bind the active layer to the RDE tip. The advantage of these RDE-based techniques over the GDE lies in the fact that (i) they require small amount of electroactive material, (ii) enable facile correction from mass-transport limitations and (iii) employ comparable ink composition than in PEMFC electrodes. However, it should be pointed out that the use of a binder (*i.e.* Nafion® for PEMFC purposes) is mandatory, thus emphasizing a drawback of the RDE: the intrinsic activity of the Pt/C or PtM/C materials is always quantified in the presence of a dual electrolyte, Nafion® + H_2SO_4 (or $HClO_4$). In that frame, one may wonder if the electrocatalytic activities monitored in such setups match those monitored only at the interface with (i) liquid electrolyte and (ii) polymer electrolyte. While question (ii) is still not clearly answered yet (apart from reference [45], little has been done so far on the topic), Guilminot et al. [22] have unveiled some of the answers to question (i), as described below.

Comparing the results of Pt/CB (10 wt.% Pt on Vulcan XC72, E-TEK) characterization using the porous RDE and the UMEC techniques in the presence/absence of Nafion® (binder), Guilminot et al. did investigate the influence of Nafion® (ionomer) on the intrinsic catalytic activity of platinum. Their study focused on two classical techniques of characterization of Pt/CB electrocatalysts. The first is the CO-stripping voltammetry (see Fig. 5), which enables

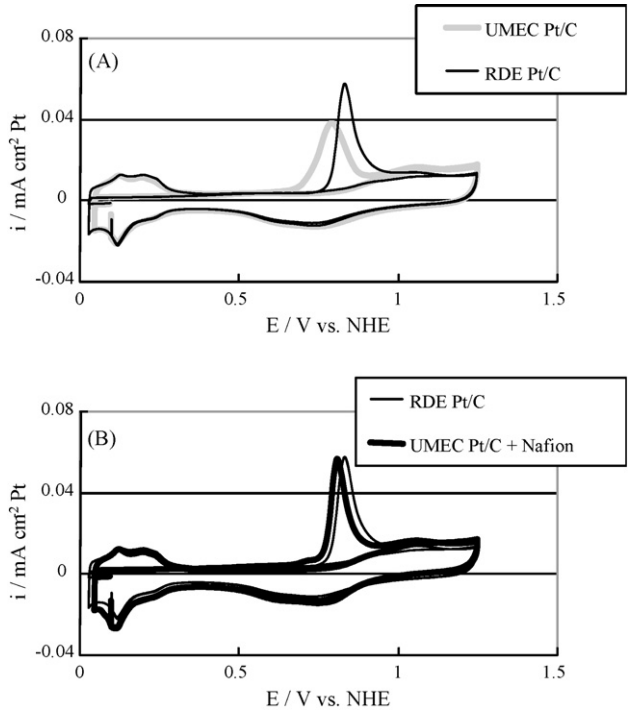

Fig. 5. Comparison of 10 mV s^{-1} CO-stripping voltammograms plotted in 1 M H_2SO_4 at 298 K for a Pt/CB active layer UMEC including or not recast Nafion® and RDE active layer (containing Nafion®).

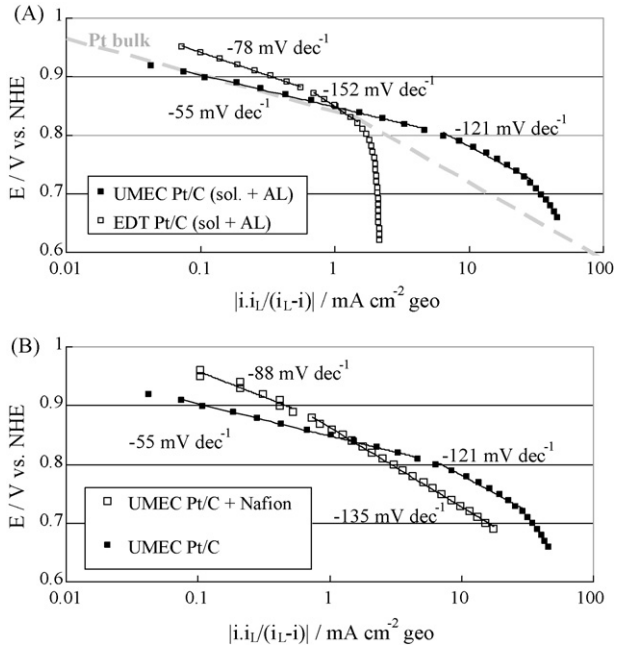

Fig. 6. (A) ORR Tafel slopes for a Pt/CB porous RDE and UMEC including recast Nafion® and (B) for a Pt/CB active layer UMEC containing or not recast Nafion® – ORR Tafel slopes obtained after correction from the diffusion in the solution and in the active layer. Reproduced from Ref. [22] with permission from Elsevier. Grey dotted line for Pt_{bulk} re-plotted from reference [62].

both quantitative determination of the active area of platinum [55] and qualitative information regarding the structure of the platinum nanoparticles, *e.g.* the existence of families of particles with different average diameter [13,14,56] and the extent of particle agglomeration [57]. The second is the quasi-steady-state voltammetry of oxygen reduction reaction (ORR) (see Fig. 6), so as to obtain the kinetic parameters of the electrocatalyst.

Fig. 5A shows that the CO-stripping peak of the Pt/CB UMEC (without Nafion®) sharply differs from that of the porous RDE (with Nafion®): both the onset and peak potentials are shifted positive when Nafion® is employed. The rationale for such differences was explained by the presence of (mainly organic) impurities brought by the Nafion® ionomer or the competitive adsorption between Nafion® sulfonate pending moieties and water, which both hinder the "water activation" step necessary for CO electrooxidation [22]. Indeed, it is well-established that CO-electrooxidation proceeds according to the Langmuir–Hinshelwood (L–H) mechanism [58] and involves the reversible adsorption of water (Eq. (1)) and the electrooxidation of adsorbed carbon monoxide with adsorbed water (Eq. (2)):

$$H_2O \leftrightarrow OH_{ads} + H^+ + e^- \quad (1)$$

$$CO_{ads} + OH_{ads} \rightarrow CO_2 + H^+ + e^- \quad (2)$$

Water splitting is known to initiate at some active sites of the surface (Eq. (1)) and provides oxygenated species which are necessary for $CO_{ads} + OH_{ads}$ recombination and CO_2 formation (Eq. (2)). At the onset of CO_{ads} electrooxidation, the reaction is limited by reactions 1 and 2 [59]. A decrease of the number of catalytic sites due to competitive adsorption between water and organic impurities or sulfonate pending moieties yields lower reaction rate for Eq. (1) and this translates in the CV by a shift of both the onset and main electrooxidation peak to higher potentials. When a Pt/CB + Nafion® blend is immobilized in the UMEC, the RDE and UMEC responses are similar, both in terms of onset and peak potentials (Fig. 5B). This finding demonstrates that the differences monitored in the Nafionless UMEC and the RDE configurations do not originate from any "electrode setup" effect, but are related only to the presence of the Nafion® ionomer.

These results agree with those from reference [60] regarding the effect of the halide and Nafion® pollutants on CO-stripping. They also agree with the lower CO to hydrogen coulometry ratios for Nafionless UMEC active layers ($Q_{CO}/Q_H \approx 2.2$) compared to those containing Nafion® ($Q_{CO}/Q_H \approx 2.8$ for the UMEC with Nafion® and 2.6 for the porous RDE). We point out that Q_{CO}/Q_H should be equal to 2 for polycrystalline Pt.[4]

Fig. 6A shows the marked difference between the diffusion-corrected[5] ORR Tafel slopes for the Pt/CB UMEC and porous RDE. Let us note that only the trace for the Pt/CB UMEC is close to that theoretically forecast for Pt (Damjanovic mechanism with Tafel slopes of −60 and −120 mV dec^{-1} at low and high ORR overpotentials, respectively [61]) and that measured for bulk Pt [62]. Conversely, the trace for the Pt/CB + Nafion® UMEC is very close to the porous RDE (Fig. 6B), showing once again the non-negligible influence of Nafion®. In the present case, the effect is dual. On the one hand, the positive effect of Nafion® on the ORR kinetics at high potentials is a consequence of the higher acidity of Nafion® (a superacid species), which shifts the ORR equilibrium potential positive and accelerates the rate-determining step of the ORR [63]. On the other hand, the Tafel slopes are always steeper and poorly defined with Nafion®, as a result of the higher O_2 mass-transport limitations in the electrolyte-soaked Nafion® (in both the RDE and UMEC configurations, O_2 is dissolved into the acid liquid electrolyte, the diffusion of which in the flooded active layer is hindered) [22]. Recently, Neyerlin at al. also showed that, in PEMFC, uncorrected O_2 mass-transport hindrance yields to higher (and poorly-defined) ORR Tafel slopes [49]. In summary, the Tafel slopes monitored for Pt/CB nanoparticles should not differ from that predicted for bulk platinum, *i.e.* −60 and −120 mV dec^{-1} at low and high ORR overpotential, respectively. Thus, the higher absolute values of the first Tafel slope (the Tafel slope measured at low current density) commonly found in the literature in the RDE or GDE setup (see for example references [15,38,44,63,64]) probably translates insufficient correction from O_2 mass-transport hindrance within the liquid-electrolyte-soaked Nafion®-containing active layers used in these studies.

3.4. Interaction between the PEM/ionomer and electrocatalyst and its impact on the MEA durability

One of the main hindrances to PEMFC commercialization is their lack of durability, as revealed by the increasing amount of literature dealing with the topic (the interested reader is directed towards relevant reviews in the field, among which [4,65–67]). As pointed out recently in [66,68], the degradation processes occurring within a PEMFC MEA during its ageing are complex, and the degradation of the PEM/ionomer and that of the Pt/C electrocatalyst are possibly linked [68–70]. On the one hand, the presence of the ionomer (and its degradation by-products) at the interface with the electrocatalyst particles affects the stability of the Pt/C materials and thus that of the whole AL [68,69,71] while, on the other hand, the AL and its degradation products destabilize the PEM/ionomer, thereby lowering the PEMFC performance and durability.

[4] Maillard et al. recently showed that this assertion could prove erroneous for platinum nanoparticles of diameter below 3–4 nm [14]. However in the present case, the fact that Q_{CO}/Q_H increases in the presence of Nafion® at fixed Pt particles diameter (the Pt/C used remains unchanged for all the experiments) unambiguously reveals the effect of the pollutants brought by Nafion® on the measurement of the active area of Platinum.

[5] Both the UMEC and the porous RDE techniques require the correction from the oxygen diffusion in the active layer for high ORR overpotentials ($E < 0.8$ V *vs.* NHE). At low ORR overpotential ($E > 0.8$ V *vs.* NHE) only the UMEC requires a correction from the oxygen diffusion in the active layer (see Section 2.4).

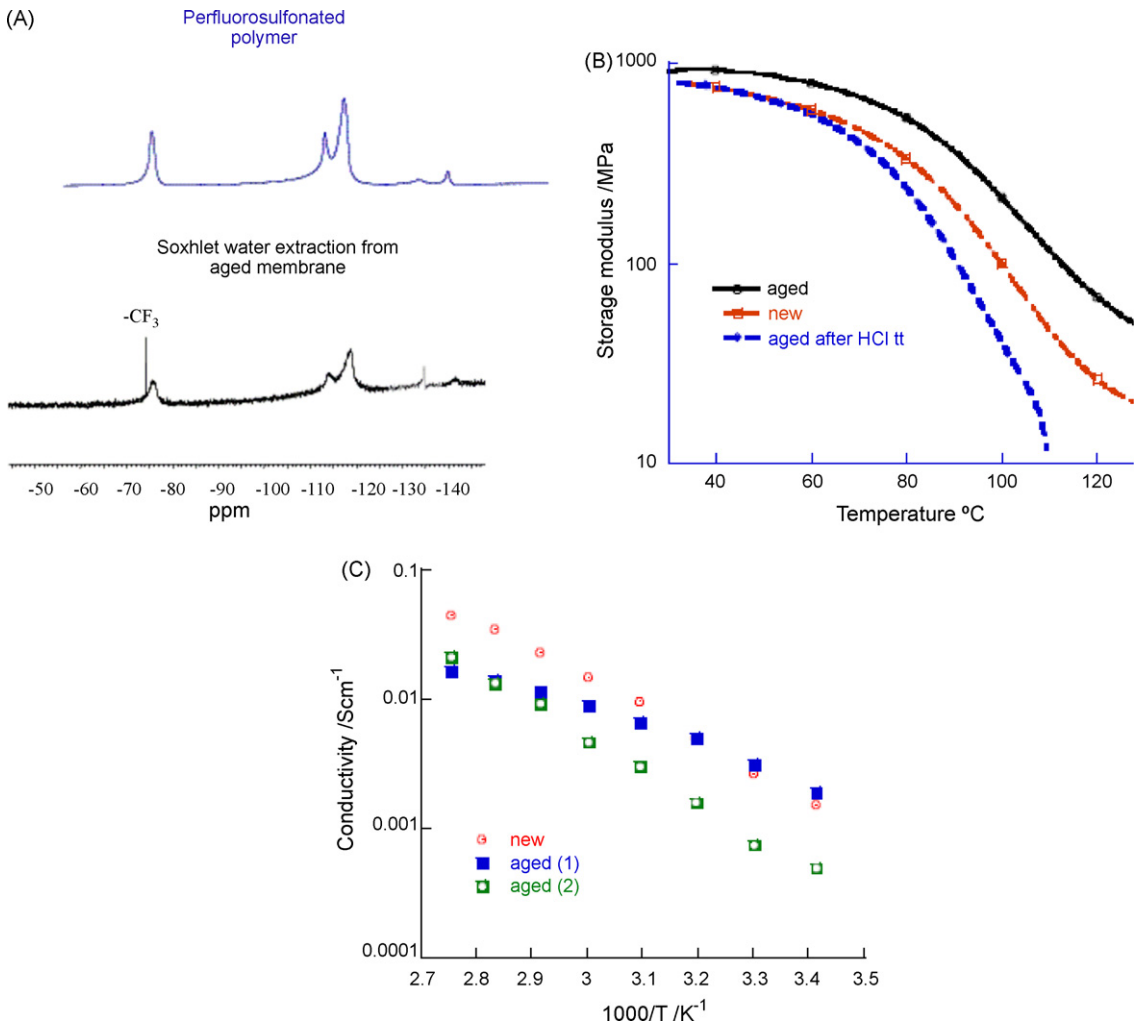

Fig. 7. (A) ^{19}F NMR spectra of Soxhlet water extraction of an aged MEA and reference for a new PEM dissolved in water/ethanol mixture. (B) Storage tensile modulus *vs.* temperature at 1 Hz for new and aged MEA before and after HCl treatment. (C) Proton conductivities (measured from electrochemical impedance spectroscopy, EIS) for new and aged MEA. 98 RH%, (1) first heat-up; (2) second heat-up. Reproduced from Ref. [71] with permission from the Electrochemical Society.

Obviously, the Pt/C electrocatalyst commonly used in PEMFC MEA is not a stable material in the PEMFC environment. For example, the thermodynamically stable form of platinum is Pt cations in the domain of pH < 1 and $E > 0.9$ V *vs.* NHE [72]. Such conditions may appear harsh, but constitute the working environment of a PEMFC cathode under small load or open-circuit voltage (OCV).[6] The corrosion of the Pt crystallites and concomitant production of Pt^{z+} is actually activated by the potential but needs a chemical step (dissolution of PtO oxides) to proceed, as suggested by Darling and Meyers [74]. It is worth noting that the presence of the (cation-exchange) ionomer/membrane provides activators for Pt^{z+} dissolution. Pt oxidation and subsequent dissolution yields the formation of a supersaturated Pt^{z+} solution at the cathode. These Pt^{z+} ions might form stable complexes with membrane/ionomer degradation products (F or S-containing species [70,75–77], see Fig. 7A), halide species arising from the Pt nanoparticles synthesis (*e.g.* Cl^- [69]) or present as impurities onto the high-surface-area carbon black substrate of the Pt nanoparticles [68,69]. As a result, Pt species redistribute within the whole MEA. In addition, the carbon support is also unstable in the environment of a PEMFC cathode. It may oxidize to CO_2 in chemical/electrochemical processes involving protons (provided by the PEM and the ionomer) [78–81]. Carbon corrosion is seemingly catalyzed by the presence of platinum [82] and depends on the electrode potential and the system operating parameters (*e.g.* start/stops, fuel starvation, OCV holds, etc.) [65]. Detailing the consequences of such degradation of the Pt/C electrocatalysts is beyond the scope of the present paper, but it is obvious that such phenomena would yield severe performance losses through the drastic reduction of u_{Pt} and ε, the morphology of both the electrocatalyst and the AL being deeply modified (see for example [65,66]).

Alternatively, the PEMFC ageing issue can be regarded from another viewpoint: the PEM and ionomer may precisely degrade as a result of the presence of the two AL in the PEMFC environment. It is now well documented that the main chemical degradation mechanism of a PFSI ionomer results from the action of radical species, like $OH^\bullet$ and $HO_2^\bullet$ [83,84]. These radicals likely originate either from the oxygen crossover through the PEM (which is especially likely for a degraded PEM) and subsequent two-electron oxygen reduction at the Pt/C anode catalyst [85], or from oxygen reduction on contaminated Pt/C cathode catalyst (*e.g.* in presence of metal cations originating from the degradation of the bipolar plates) [86,87].

[6] Obviously, in non-electrochemical CMR baring a Nafion® membrane, Pt-based catalysts could also suffer such Pt corrosion since, by nature, non-electrochemical CMR operate in open circuit conditions. Should such CMR be exposed to both a strong reducer and a strong oxidant (an example is given in reference [73], the oxidant compartment open-circuit potential could reach ca. 1 V vs. NHE, yielding dissolution of the Pt catalyst. The phenomenon would be even harsher for catalysts less noble than platinum.

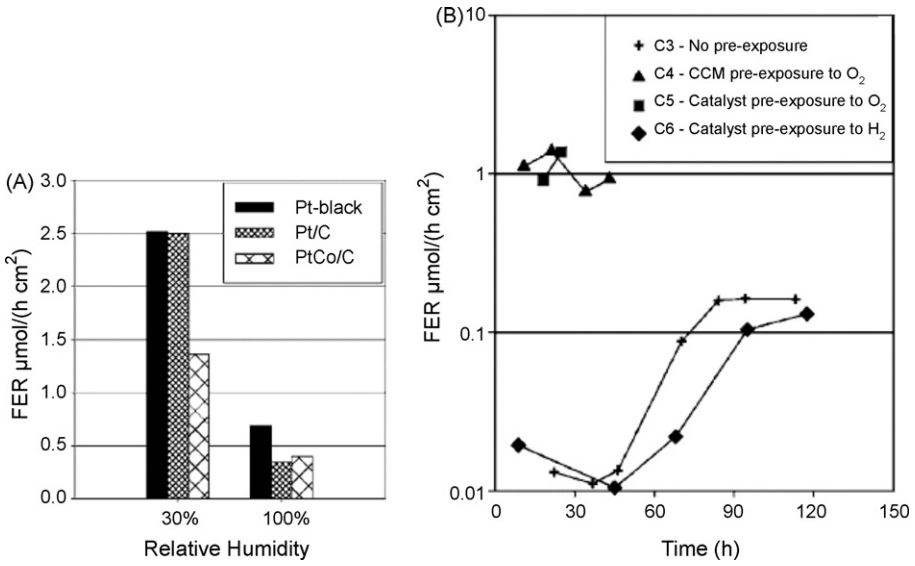

Fig. 8. (A) Total Fluoride Emission Rate (FER) from standard cells with Nafion 117 membrane and Pt-black, Pt/C, and PtCo/C (C = carbon black) as the catalysts. Both anode and cathode of the standard cells were made with the same catalyst type. The cells were tested at 90 °C, with H_2 and O_2 as the reactant gases at OCV and at RH = 30 or 100%. (B) Total FER from bilayer membrane cells tested at 90 °C, 30 RH% with H_2 and O_2 as the reactant gases. The thin catalyst layer sandwiched between the Nafion 117 and Nafion 112 membrane in the bilayer membrane cells had different test histories. From Ref. [88] with permission from the Electrochemical Society.

In that context, the polarization of the electrode that exists in a PEMFC is obviously a key parameter for the observed extent and rate of degradation: the degradation of the PEM ionomer is especially likely in the vicinity of the anode, as detailed in recent review articles [66,84,86]. The nature of the electrocatalyst (Fig. 8A) and atmosphere (Fig. 8B) also affects the degradation rate of the PEM, as recently demonstrated by Mittal et al. [88]. It is interesting to note that Mittal et al. measured comparable membrane degradation rates irrespective of the location of the Pt/C catalyst (anode, cathode or in the membrane), which they relate to an independence of the reaction to the electrode potential, thus asserting its chemical nature. This conclusion differs from the previous one, but can be understood as follows: the (electrode) potential may not have a direct effect on the PEM/ionomer degradation, but instead on the formation of species (*e.g.* Pt^{z+}, radicals, etc.), which influences the degradation of the PEM. Let us recall that the presence of Pt^{z+} species in the PEM/ionomer alters its bulk properties: ion-exchange capacity, water uptake, mechanical strength, etc. (Fig. 7B), and its proton conductivity (Fig. 7C) [66,70,71,86,89], finally concurring to a decrease of the PEMFC performance. Nevertheless, from that prospect, the PEM/ionomer degradation might as well proceed in non-electrochemical CMR, *e.g.* systems in which H_2O_2 (a species likely prone to radical formation) is used as the oxidant (see examples in references [73,90]).

4. Conclusion

In the present paper, through a selected literature review, we compared the Proton Exchange Membrane Fuel Cells (PEMFC) to Catalytic Membrane Reactors (CMR). On the one hand, we showed that PEMFC and CMR display major differences in terms of operating conditions. In particular, each active layer (AL) of the PEMFC membrane electrode assembly (MEA) operates at a defined electrode potential, thereby translating a major difference between PEMFC and non-electrochemical CMR. Consequently, in opposition to what happens in non-electrochemical CMR (for which the catalysts operate in open-circuit conditions), the electrochemical reactions taking place in PEMFC can only occur at the so-called three-phase-boundaries between the carbon-supported electrocatalyst particles and the ionomer, in the presence of the reactants. On the other hand, PEMFC are particular (electrochemical) CMR. As such, the PEMFC and CMR also display a certain number of similarities, notably in terms of materials used and system geometry.

Like non-electrochemical CMR, PEMFC only reach high performances provided the MEA is based on efficient materials and properly designed. The MEA is a complex medium, composed of a Proton Exchange Membrane (PEM), two active layers and two gas diffusion layers (GDL). The PEM acts as both electron and gas separator between the anode and cathode active layers and transport medium for protons (*extractor* at the anode, *distributor* at the cathode). Each AL of the PEMFC MEA is a CMR where the ionomer acts as a *distributor* for protons (cathode) and dissolved gases, *contactor* between the gas reactant, protons and electrocatalyst particles and *extractor* for the reaction by-products (H^+ at the anode, H_2O at the cathode).

Obviously in a running PEMFC, each AL operates at a relevant potential that depends on the reaction (ORR or HOR), therefore rendering necessary the existence of optimized three-phase boundaries (reactant|ionomer|electrocatalyst interface). We showed that the performances of practical PEMFC MEA improved thanks to the optimization of the ionomer|electrocatalyst interface, yielding to better electrocatalyst *utilization* and *effectiveness* factors. Conversely, such three-phase boundaries are not mandatory in non-electrochemical CMR, in which the catalytic reactions are not achieved under potential control. We showed that an unexpected consequence of the required intimate contact between the ionomer and the electrocatalyst, is the modification of the intrinsic activity of the Pt-based electrocatalysts: the presence of Nafion® indeed modifies the environment of the Pt particle (as compared to the gas or liquid electrolyte phase), *e.g.* due to adsorption of ionomer moieties, pollution or pH variation.

Finally, we emphasized that the MEA architecture/composition influences its durability. Briefly, C oxidizes to CO_2 and Pt dissolves in the acidic and oxidant environment of the PEMFC cathode, yielding Pt^{z+} ion release and transport within the MEA. The latter is favored by the presence of the (cation-exchange) ionomer/membrane and by activators/ligands (F or S-containing species resulting from the ionomer and membrane degradation), which possibly act as counter-ions. As a result, the ageing mechanisms of both the Pt/C nanoparticles and ionomer/membrane actually depend on each other and overall, the presence of the ionomer at the interface with the electrocatalyst particles affects the stability of the whole

AL. Obviously, such degradation issues depend on the operating potential of each PEMFC AL. Non-electrochemical CMR based on a Nafion® (or any superacid) membrane, operating by nature at open-circuit potential, would also likely suffer such degradation when operated with "aggressive" reactants, because these conditions are comparable to those in PEMFC during idling or at zero current.

Acknowledgements

The authors thank Dr Sandrine Berthon-Fabry (Center for Energy and Processes, Mines ParisTech, Sophia-Antipolis) and her team for their major contribution in the studies dealing on the carbon aerogels elaboration, characterization and tests, and for testing the carbon xerogels in PEMFC unit cells. MC and FM thank the French Agence Nationale de la Recherche (ANR) for funding in the framework of the MDM (ANR-07-PANH-008-03) and Carbocell (ANR-07-MATEPRO-06-181138) projects. MC and NJ thank Egide and the WBI for funding within the project Tournesol #20389PF. NJ thanks the F.R.S.-FNRS for a postdoctoral fellowship.

References

[1] J.-A. Dalmon, in: G. Ertl, H. Knözinger, J. Weitkamp (Eds.), Catalytic Membrane Reactors, Chapter 9.3, Handbook of Heterogeneous Catalysis, Wiley, Chichester, 1997, pp. 1387–1398.
[2] R. Dittmeyer, K. Svajda, M. Reif, Top. Catal. 29 (2004) 3.
[3] W. Vielstich, A. Lamm, H.A. Gasteiger, in: W. Vielstich, A. Lamm, H.A. Gasteiger (Eds.), Handbook of Fuel Cells, vols. 1–4, Wiley, Chichester, 2003.
[4] H.A. Gasteiger, W. Vielstich, H. Yokokawa, in: H.A. Gasteiger, W. Vielstich, H. Yokokawa (Eds.), Handbook of Fuel Cells, vols. 5–6, John Wiley & Sons Ltd, Chichester, 2009.
[5] M. Mathias, J. Roth, J. Fleming, W. Lehnert, Diffusion media materials and characterisation, in: W. Vielstich, H.A. Gasteiger, A. Lamm (Eds.), Handbook of Fuel Cells, vol. 3, Wiley, Chichester, 2003, pp. 517–537.
[6] H.A. Gasteiger, S.S. Kocha, B. Sompalli, F.T. Wagner, Appl. Catal. B: Environ. 56 (2005) 9.
[7] E. Thiele, Ind. Eng. Chem. 31 (1939) 916.
[8] A. Wheeler, Adv. Catal. 3 (1951) 249.
[9] P. Stonehart, P.N. Ross, Electrochim. Acta 21 (1976) 441.
[10] F. Gloaguen, F. Andolfatto, R. Durand, P. Ozil, J. Appl. Electrochem. 24 (1994) 863.
[11] G.F. Froment, K.B. Bischoff, in: G.F. Froment, K.B. Bischoff (Eds.), Chemical Reactor Analysis and Design, 2nd ed., Wiley, New York, 1990.
[12] S.S. Kocha, Principle of MEA preparation, in: W. Vielstich, A. Lamm, H.A. Gasteiger (Eds.), Principle of MEA Preparation, Handbook of Fuel Cells, vol. 3, Wiley, Chichester, 2003, pp. 538–565.
[13] F. Maillard, S. Pronkin, E.R. Savinova, Size effects in electrocatalysis of fuel cells reactions on supported metal nanoparticles, in: M.T.M. Koper (Ed.), Fuel Cell Catalysis: a Surface Science Approach, John Wiley & Sons, Inc., New York, 2009, pp. 507–566.
[14] F. Maillard, S. Pronkin, E.R. Savinova, Influence of size on the electrocatalytic activities of supported metal nanoparticles in fuel cells related reactions, in: W. Vielstich, H.A. Gasteiger, H. Yokokawa (Eds.), Handbook of Fuel Cells, vol. 5, John Wiley & Sons, Inc., New York, 2009, pp. 91–111.
[15] U.A. Paulus, T.J. Schmidt, H.A. Gasteiger, R.J. Behm, J. Electroanal. Chem. 495 (2001) 134.
[16] T.J. Schmidt, H.A. Gasteiger, R.J. Behm, J. Electrochem. Soc. 146 (1999) 1296.
[17] T.J. Schmidt, H.A. Gasteiger, G.D. Stab, P.M. Urban, D.M. Kolb, R.J. Behm, J. Electrochem. Soc. 145 (1998) 2354.
[18] A. Gamez, D. Richard, P. Gallezot, F. Gloaguen, R. Faure, R. Durand, Electrochim. Acta 41 (1996) 307.
[19] A.J. Bard, L.R. Faulkner, Electrochemical Methods, John Wiley & Sons, Inc., Weinheim, 2001.
[20] F. Gloaguen, R. Durand, J. Appl. Electrochem. 27 (1997) 1029.
[21] O. Antoine, Y. Bultel, R. Durand, P. Ozil, Electrochim. Acta 43 (1998) 3681.
[22] E. Guilminot, A. Corcella, M. Chatenet, F. Maillard, J. Electroanal. Chem. 599 (2007) 111.
[23] M. Chatenet, in: V. Vivier (Ed.), L'ultramicroélectrode à cavité (UMEC) en électrocatalyse – principe, exemples et difficultés expérimentales, Microélectrode à cavité – Principe, développement et applications d'un outil pour l'étude de la réactivité de matériaux insolubles, Presses Universitaires de Saint-Etienne, Saint-Etienne, 2009, pp. 75–97.
[24] I. Roche, E. Chainet, M. Chatenet, J. Vondrak, J. Phys. Chem. C 111 (2007) 1434.
[25] J.M. Song, S. Suzuki, H. Uchida, M. Watanabe, Langmuir 22 (2006) 6422.
[26] G. Bender, T.A. Zawodzinski, A.P. Saab, J. Power Sources 124 (2003) 114.
[27] A.P. Saab, F.H. Garzon, T.A. Zawodzinski, J. Electrochem. Soc. 150 (2003) A214.
[28] H. Xu, E.L. Brosha, F.H. Garzon, F. Uribe, M. Wilson, B. Pivovar, ECS Trans. 11 (2007) 383.
[29] E. Brosha, J. Chlistunoff, F. Garzon, B. Orler, B. Pivovar, C. Welch, D. Wrobleski, H. Xu, HFCIT merit review, Department of Energy Arlington, Virginia, June 2008.
[30] K. More, R. Borup, K. Reeves, ECS Trans. 3 (2006) 717.
[31] V. Rao, P.A. Simonov, E.R. Savinova, G.V. Plaksin, S.V. Cherepanova, G.N. Kryukova, U. Stimming, J. Power Sources 145 (2005) 178.
[32] E. Antolini, L. Giorgi, A. Pozio, E. Passalacqua, J. Power Sources 77 (1999) 136.
[33] J.M. Song, S.Y. Cha, W.M. Lee, J. Power Sources 94 (2001) 78.
[34] G. Li, P.G. Pickup, J. Electrochem. Soc. 150 (2003) C745.
[35] H.A. Gasteiger, J.E. Panels, S.G. Yan, J. Power Sources 127 (2004) 162.
[36] S. Litster, G. McLean, J. Power Sources 130 (2004) 61.
[37] N. Job, J. Marie, S. Lambert, S. Berthon-Fabry, P. Achard, Energy Convers. Manag. 49 (2008) 2461.
[38] J. Marie, S. Berthon-Fabry, P. Achard, M. Chatenet, A. Pradourat, E. Chainet, J. Non-Cryst. Solids 350 (2004) 88.
[39] R.W. Pekala, J. Mater. Sci. 24 (1989) 3221.
[40] N. Job, R. Pirard, J. Marien, J.P. Pirard, Carbon 42 (2004) 619.
[41] N. Job, A. Théry, R. Pirard, J. Marien, L. Kocon, J.-N. Rouzaud, F. Béguin, J.-P. Pirard, Carbon 43 (2005) 2481.
[42] J. Marie, R. Chenitz, M. Chatenet, S. Berthon-Fabry, N. Cornet, P. Achard, J. Power Sources 190 (2009) 423.
[43] J. Marie, S. Berthon-Fabry, P. Achard, M. Chatenet, E. Chainet, R. Pirard, N. Cornet, ECS Trans. 1 (2006) 509.
[44] J. Marie, S. Berthon-Fabry, M. Chatenet, E. Chainet, R. Pirard, N. Cornet, P. Achard, J. Appl. Electrochem. 37 (2007) 147.
[45] M. Umeda, T. Maruta, M. Inoue, A. Nakazawa, J. Phys. Chem. C 112 (2008) 18098.
[46] N. Job, B. Heinrichs, S. Lambert, J.-P. Pirard, J.-F. Colomer, B. Vertruyen, J. Marien, AIChE J. 52 (2006) 2663.
[47] M. Uchida, Y. Fukuoka, Y. Sugawara, N. Eda, A. Ohta, J. Electrochem. Soc. 143 (1996) 2245.
[48] F. Maillard, P. Simonov, E.R. Savinova, Carbon materials as support for fuel cells electrocatalysts, in: P. Serp, J.L. Figueiredo (Eds.), Carbon Materials for Catalysis, vol. 5, John Wiley & Sons, Inc., New York, 2009, pp. 429–480.
[49] K.C. Neyerlin, W. Gu, J. Jorne, A. Clark, H.A. Gasteiger, J. Electrochem. Soc. 154 (2007) B279.
[50] L. Genies, R. Faure, R. Durand, Electrochim. Acta 44 (1998) 1317.
[51] M. Chatenet, L. Genies-Bultel, M. Aurousseau, R. Durand, F. Andolfatto, J. Appl. Electrochem. 32 (2002) 1131.
[52] M. Chatenet, M. Aurousseau, R. Durand, F. Andolfatto, J. Electrochem. Soc. 150 (2003) D47.
[53] L. Genies, Y. Bultel, R. Faure, R. Durand, Electrochim. Acta 48 (2003) 3879.
[54] J. Vondrak, B. Klapste, J. Velicka, M. Sedlarikova, J. Reiter, I. Roche, E. Chainet, J.F. Fauvarque, M. Chatenet, J. New Mater. Electrochem. Syst. 8 (2005) 209.
[55] K. Shinozaki, T. Hatanaka, Y. Morimoto, ECS Trans. 11 (2007) 497.
[56] F. Maillard, M. Eikerling, O.V. Cherstiouk, S. Schreier, E. Savinova, U. Stimming, Faraday Discus. 125 (2004) 357.
[57] F. Maillard, S. Schreier, M. Hanzlik, E.R. Savinova, S. Weinkauf, U. Stimming, Phys. Chem. Chem. Phys. 7 (2005) 385.
[58] S. Gilman, J. Phys. Chem. 68 (1964) 70.
[59] B. Andreaus, F. Maillard, J. Kocylo, E.R. Savinova, M. Eikerling, J. Phys. Chem. B 110 (2006) 21028.
[60] D. Strmcnik, A. Gaberscek, S. Hocevar, J. Jamnik, Solid State Ionics 176 (2005) 1759.
[61] A. Damjanovic, V. Brusic, Electrochim. Acta 12 (1967) 615.
[62] D. Chu, S. Gilman, J. Electrochem. Soc. 141 (1994) 1770.
[63] O. Antoine, Y. Bultel, R. Durand, J. Electroanal. Chem. 499 (2001) 85.
[64] F. Maillard, M. Martin, F. Gloaguen, J.M. Léger, Electrochim. Acta 47 (2002) 3431.
[65] F.A. de Bruijn, V.A.T. Dam, G.J.M. Janssen, Fuel Cells 8 (2008) 3.
[66] M. Chatenet, L. Guétaz, F. Maillard, Electron microscopy to study MEA materials and structure degradation, in: H.A. Gasteiger, W. Vielstich, H. Yokokawa (Eds.), Handbook of Fuel Cells, vol. 6, John Wiley & Sons, Chichester, 2009, pp. 844–860.
[67] R. Borup, J. Meyers, B. Pivovar, Y.S. Kim, R. Mukundan, N. Garland, D. Myers, M. Wilson, F. Garzon, D. Wood, P. Zelenay, K. More, K. Stroh, T. Zawodzinski, J. Boncella, J.E. McGrath, M. Inaba, K. Miyatake, M. Hori, K. Ota, Z. Ogumi, S. Miyata, A. Nishikata, Z. Siroma, Y. Uchimoto, K. Yasuda, K.I. Kimijima, N. Iwashita, Chem. Rev. 107 (2007) 3904.
[68] E. Guilminot, A. Corcella, C. Iojoiu, G. Berthomé, F. Maillard, M. Chatenet, J.-Y. Sanchez, J. Electrochem. Soc. 154 (2007) B1106.
[69] E. Guilminot, A. Corcella, F. Charlot, F. Maillard, M. Chatenet, J. Electrochem. Soc. 154 (2007) B96.
[70] C. Iojoiu, E. Guilminot, F. Maillard, M. Chatenet, J.Y. Sanchez, E. Claude, E. Rossinot, J. Electrochem. Soc. 154 (2007) B1115.
[71] M. Chatenet, E. Guilminot, C. Iojoiu, J.-Y. Sanchez, E. Rossinot, F. Maillard, ECS Trans. 11 (2007) 1203.
[72] M. Pourbaix, Atlas of Electrochemical Equilibria in Aqueous Solutions, National Association of Corrosion Engineers, Houston, 1979, p. 453.
[73] C. Espro, F. Arena, F. Tasselli, A. Regina, E. Drioli, A. Parmaliana, Catal. Today 118 (2006) 253.
[74] R.M. Darling, J.P. Meyers, J. Electrochem. Soc. 150 (2003) A1523.
[75] J. Healy, C. Hayden, T. Xie, K. Olson, R. Waldo, A. Brundage, H. Gasteiger, J. Abbott, Fuel Cells 5 (2005) 302.
[76] J. Xie, D.L. Wood, K.L. More, P. Atanassov, R.L. Borup, J. Electrochem. Soc. 152 (2005) A1011.
[77] J. Xie, D.L. Wood, D.M. Wayne, T.A. Zawodzinski, P. Atanassov, R.L. Borup, J. Electrochem. Soc. 152 (2005) A104.
[78] K.H. Kangasniemi, D.A. Condit, T.D. Jarvi, J. Electrochem. Soc. 151 (2004) E125.
[79] K. Kinoshita, Influence of heat treatment and physicochemical properties on the electrochemical oxidation of carbon blacks in phosphoric acid Proceedings of

the Workshop on the Electrochemistry of Carbon, vols. 84–85, The Electrochem. Soc., Inc., Pennington, 1984, p. 273.
[80] K. Kinoshita, Carbon, Electrochemical and Physicochemical Properties, John Wiley & Sons, New York, 1988.
[81] K. Kinoshita, J. Bett, Carbon 11 (1973) 237.
[82] L.M. Roen, C.H. Paik, T.D. Jarvi, Electrochem, Solid State Lett. 7 (2004) A19.
[83] A. Laconti, H. Liu, C. Mittelsteadt, R. McDonald, ECS Trans. 1 (2006)199.
[84] A.B. Laconti, M. Hamdan, R.C. McDonald, Mechanisms of membrane degradation, in: W. Vielstich, A. Lamm, H.A. Gasteiger (Eds.), Handbook of Fuel Cells, vol. 3, Wiley, Chichester, 2003, pp. 647–662.
[85] O. Antoine, R. Durand, J. Appl. Electrochem. 30 (2000) 839.
[86] T. Okada, Effect of ionic contaminants, in: W. Vielstich, A. Lamm, H.A. Gasteiger (Eds.), Handbook of Fuel Cells, Vol.3, Wiley, Chichester, 2003, pp. 627–646.
[87] A.B. LaConti, H.M., R.C. McDonald, Mechanism of membrane degradation, 2003.
[88] V.O. Mittal, H.R. Kunz, J.M. Fenton, J. Electrochem. Soc. 153 (2006) A1755.
[89] T. Okada, Y. Ayato, M. Yuasa, I. Sekine, J. Phys. Chem. B 103 (1999) 3315.
[90] S.S. Ozdemir, M.G. Buonomenna, E. Drioli, Appl. Catal. A: Gen. 307 (2006) 167–183.
[91] E. Billy, F. Maillard, A. Morin, L. Guetaz, F. Emieux, C. Thurier, P. Doppelt, S. Donet, S. Mailley, Impact of ultra-low Pt loadings on the performance of anode/cathode in a Proton Exchange Membrane Fuel Cell, J. Power Sources 195 (2010) 2737–2746.